UDC 539.4

Study on the Fabrication of Nano-SiC/Ni-P Composite Coatings with the Assistance of Electromagnetic-Ultrasonic Compound Field

H. Z. Zhou,[a,b,1] W. H. Wang,[b] Y. Q. Gu,[b] X. X. Fang,[a,b] and Y. Q. Bai[a,b]

[a] Jiangsu Key Laboratory of Advanced Structural Materials and Application Technology, Nanjing, Jiangsu, China

[b] Department of Material Engineering, Nanjing Institute of Technology, Nanjing, Jiangsu, China

[1] zhzmsc@njit.edu.cn

Electroless nanocomposite platings were fabricated while the magnetic field strength and ultrasonic parameters were controlled. The effect of the complex field on the composite platings' deposition process was discussed. The results show that composite coatings fabricated by a complex magnetic field had better density and homogeneity than coatings processed without the influence of external fields. The time-step deposition discussions indicate that the extra magnetic field accelerates the motion of the composite particulates in the bath through the action of the Lorentz force and promotes the nucleation and growth process of composite particulate clusters. The mechanical energy generated by the ultrasonic vibration activates the substrate surface and promotes the deposition of the Ni^{2+} in the plating solution on the substrate surface. While the complex field is functioning, ultrasonic and magnetic interactions play an important role in the fabrication of the uniform and dense nano-SiC/Ni-P composite coatings, which consist of amorphous spherical Ni-P/SiC particle clusters with 200 nm diameter. The nanoindentation hardness of these composite coatings was approximately 0.15 GPa.

Keywords: electroless composite plating, magnetic field, ultrasonic wave.

Introduction. Nanocomposite coatings have excellent properties such as high hardeness and toughness, good wear resistance and corrosion resistance by incorporating nanoparticles like $A1_2O_3$ [1, 2], MoS_2 [3], and SiC [4]. These coatings have broad application prospects in many fields, such as mechanical, aerospace, and transportation [5]. However, the traditional process of plating electroless composites often results in unstable solutions, inefficient deposition, and higher processing temperatures. In order to improve the traditional process, new preparation technologies have been invented. Niksefat and Ghorbani [6] used an ultrasonic assisted electroless plating method to prepare Ni-B-TiO_2 composite coatings with excellent performance. The same method was improved by Luo et al. [7] and Lu [8]. Zhong [9] applied the laser induced method to fabricate Ni-P/nano C60 on the surface of a smooth component. The composite coatings possessed small friction coefficients and high wear resistance. Wang et al. [10] found that the deposition efficiency of the composite coating was significantly increased in a 10 T parallel strong magnetic field. Zhao et al. [2] successfully adopted the mechanical vibration assisted electroless composite plating method to obtain multi walled carbon nanotubes reinforced with Ni-P matrix composites coatings on the carbon steel surface, while Mehto and Pandey [11] prepared copper based nanocomposite films with the same method.

In the electroless composite plating process, the introduced ultrasonic wave fields have the effect of dispersing the solution system and increasing the reaction rate. In addition, the presence of an electromagnetic field improves the deposition, nucleation, growth velocity and compactness of the coating. At present, there are only a few reports globally about the study of chemical composite plating technology with the help of an ultrasound wave and magnetic field. Therefore, this work intends to explore the effect of an electromagnetic-ultrasonic complex field on the plating of electroless nanocomposite

coatings. Within this paper, the morphology, composition and structure of the composite coatings are analyzed, and the effect of the compound field is summarized.

1. **Experimental Process and Characterization Methods**.

1.1. ***Experimental***. The matrix sample is a single side frosted glass with a size of 10×10 mm. The sample was sensitized for 10 min in a solution (30 ml/l HCl and 30 g/l $SnCl_2$) at 50°C, and then the sample was activated for 10 min in 40 ml distilled water (0.1 g $PdCl_2$ and 2 ml HCl) at 30°C. The plating solutions were created according to the formula in Table 1. After that the solutions were stirred for 5 min by an FS-1500 ultrasonic generator. Finally, the pretreated samples were immersed in the plating solution. Table 2 shows the parameters of the SB-175 type magnetic field generator and the FS-1500 type ultrasonic generator that were used during the experiment.

1.2. ***Characterization Methods***. The coating samples' micromorphology was observed by JSM-6360LV SEM, and the composition was analyzed by GENESIS2000XMS60 EDS. The phase analysis of the coatings was carried out on a Bruker AXS D8-Advance X-ray diffraction instrument using Cu ($K\alpha$) target with an X-ray wavelength of 0.15418 nm. The acceleration voltage was 30 kV, the step size was 0.02 degrees, and the scanning speed was 1.2 °/min. The hardness of the samples was tested with a nanoindentation tester (Agilent G200). The indentation depth was 100 nm, and the loading time was 30 s.

Table 1

Solution Composition and Process Conditions of Electroless Nanocomposite Plating

Component	Parameter
$NiSO_4 \cdot 6\ H_2O$	30 g/l
$NaH_2PO_2 \cdot H_2O$	30 g/l
$Na_3C_6H_5O_7 \cdot 2H_2O$	30 g/l
CH_3COONa	20 g/l
$C_3H_6O_3$	15 ml/l
SiC ($d = 20$ nm)	1 g/l
pH	4.8

Table 2

Fabrication Process of Different Samples

Sample No.	Ultrasonic wave frequency (kHz)	Ultrasonic power (W)	Magnetic field intensity (T)	Process time (min)
1	0	0	0	50
2	0	0	0.14	50
3	20	300	0	50
4	20	300	0.14	50
5	20	300	0.21	50
6	20	300	0.39	50
7	20	300	0.58	50
8	20	300	0.70	50

2. **Composite Coatings Processed under Compound Fields**. Figure 1 shows an SEM image of the frosted glass surface, from which we can see that the glass surface appears to be an irregular undulating structure after the grinding process. This undulating morphology is beneficial to the deposition of the composite coating on the substrates.

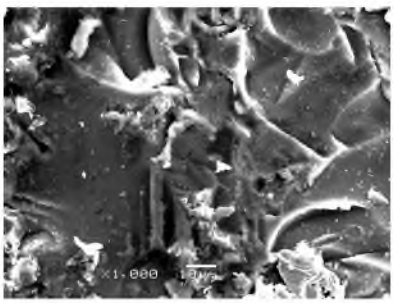

Fig. 1. SEM image of the frosted glass surface.

2.1. ***Nanocomposite Coatings Prepared under Different Additional Fields***. Figure 2 shows SEM images of the nanocomposite coating samples. As Fig. 2a shows, the surface of sample No. 1 is undulating, the gaps between particles are large, and the aggregation phenomenon is obvious. In the sample shown in Fig. 2b, which was prepared under the action of a magnetic field during the plating process, the coating is tiny and compact. This can be attributed to the tendency of Ni particles to nucleate more effectively within a magnetic field. In Fig. 2c, the aggregation of the deposited particles is not obvious, but there are still gaps. In Fig. 2d, the bottom layer of No. 4 samples is compact, and its surface consists of many spherical sediments.

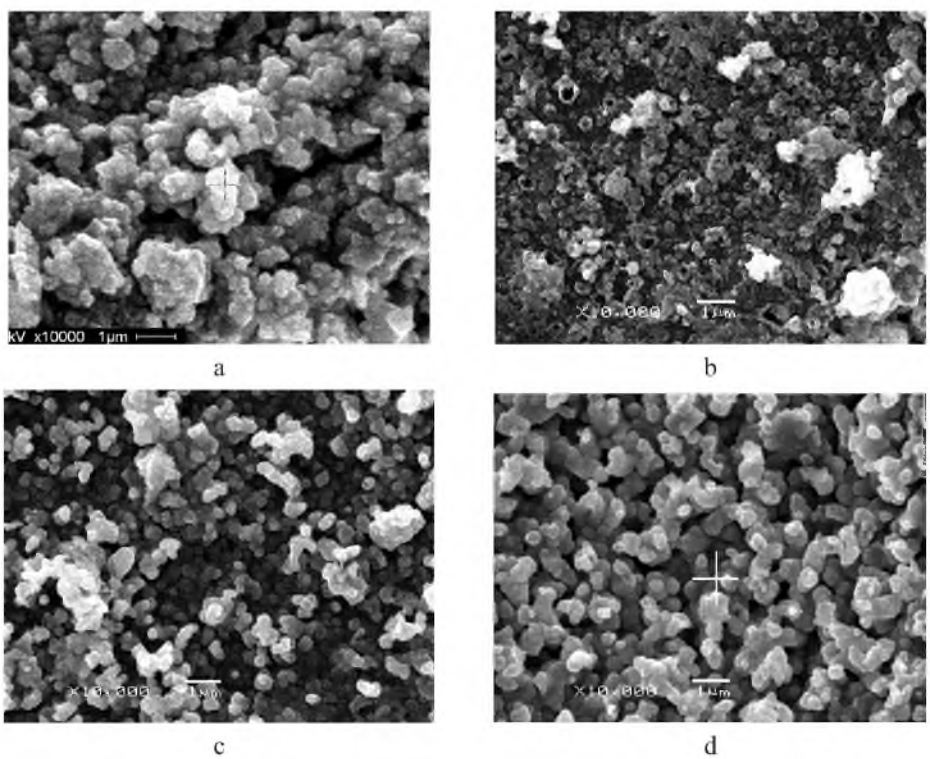

Fig. 2. SEM morphology of samples: (a) No. 1; (b) No. 2; (c) No. 3; (d) No. 4.

In general, it is difficult to create a uniform nanocomposite coating because agglomeration of nanoceramic particles [12] and aggregation of the metal nanograins [13–15] tend to occur. The experimentation in this work suggested that the aggregation phenomenon is nearly eliminated by inducing an electromagnetic-ultrasonic field, which has many implications for the applications of nanocomposite coatings.

Figure 3a and 3b contain the energy spectra analyses of the cross area on Fig. 2a and 2d. From Fig. 3a, it can be clearly seen that there are mostly Ni, P, Si, and C elements in the coating, which indicates that the composite coating is formed on the glass substrate. Na, Mg, Al, and other elements come from the glass substrate, which indicates that the composite coating is very thin. On the other hand, the mass fraction of Ni reached 63.96%, and the mass fraction of Si decreased obviously in Fig. 3b, which states clearly that the composite coating thickness is thicker. This phenomenon can be mainly attributed to increased reaction rates and acceleration of the particle groups' deposition on the glass substrate by the compound field.

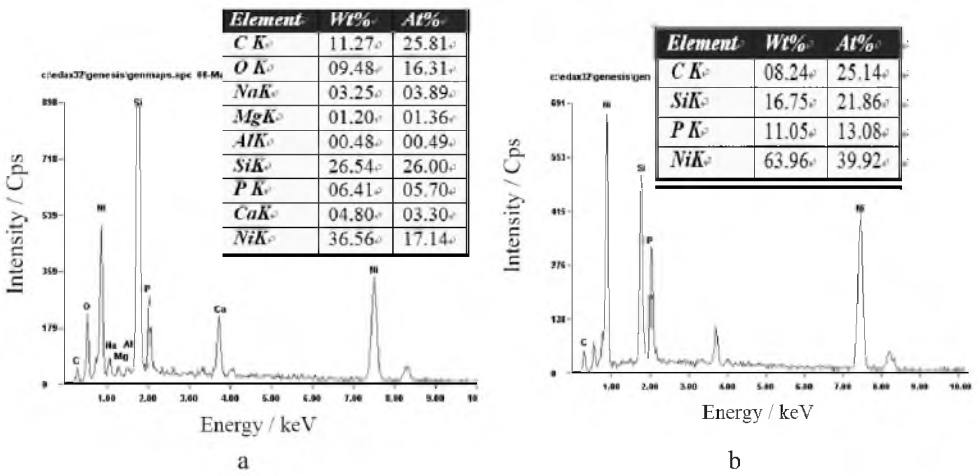

Fig. 3. EDS of samples fabricated under different additional fields: (a) No. 1; (b) No. 4.

Figure 4 gives the XRD spectra of Nos. 1–4 composite coating samples. Figure 4a and 4c show that the No. 1 and No. 3 coatings are obviously amorphous. However, the 2 theta angle of Ni at about 45 degrees manifested a weak diffraction peak in Fig. 4b and 4d, which indicates that the presence of a magnetic field in the composite plating process had an obvious effect on the nucleation and deposition of the coatings.

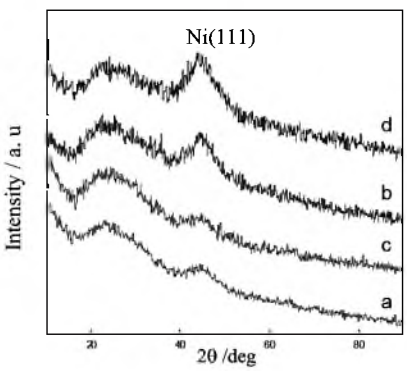

Fig. 4. XRD of composite coating samples: (a) No. 1; (b) No. 2; (c) No. 3; (d) No. 4.

2.2. ***Nanocomposite Coatings Prepared under Compound Fields***. Figure 5 shows the SEM images of Nos. 5–8 coating samples. Figure 5a–d shows that the surface of each layer is denser than that of No. 1, and the deposition of particles is obvious. As the intensity of the magnetic field increased, the coatings became more compact, and the globular trend of the deposition products became more obvious. Thus, it can be concluded that the compound field not only affected the spheroidizing of deposition products, but also promoted the densification of the composite coatings. Figure 5e gives the EDS results for the No. 8 sample. The main components of the microspherical particles in the coating are Ni, P, Si, and C. Thus, the microsphere consists of the co-deposition of Ni-P alloy and nano-SiC particles. According to the uniformity of the microsphere morphology, the distribution of SiC in the coating is also judged to be more uniform, and the SiC particles were seemingly co-deposited with Ni-P.

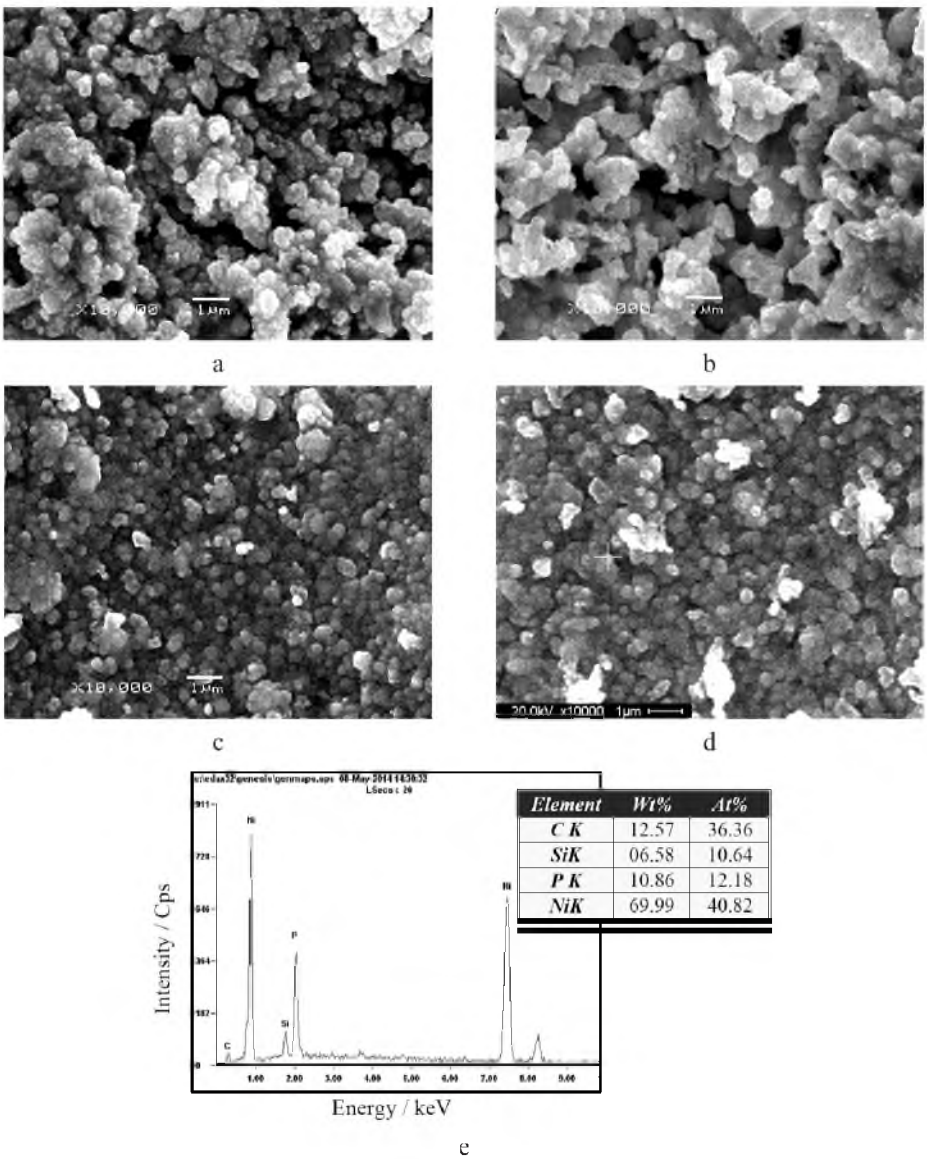

Element	*Wt%*	*At%*
C K	12.57	36.36
SiK	06.58	10.64
P K	10.86	12.18
NiK	69.99	40.82

Fig. 5. SEM morphology and EDS results: (a) No. 5; (b) No. 6; (c) No. 7; (d) No. 8; (e) EDS of the No. 8.

Figure 6 gives the section SEM image of sample No. 8. This image, along with Figs. 5c and 6, indicates that the coating on this sample is more uniform and compact. The coating also is made up of microspheres that averaged 200 nm in size. The coating thickness was approximately 7.1 μm. Furthermore, the combination between the composite coating and glass substrate was good, and the coating's morphology was independent of the matrix surface's morphology.

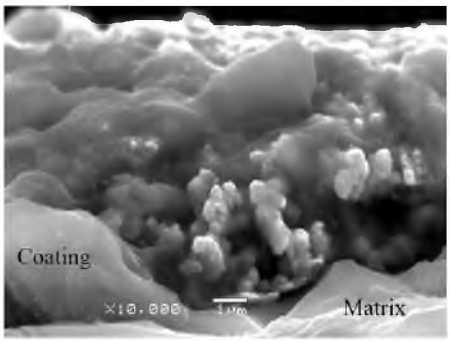

Fig. 6. Cross section SEM morphology of No. 8 sample.

Figure 7 gives XRD results of Nos. 5–8 composite coating samples. The diffraction peak in Fig. 7 leads to the conclusion that as the intensity of the magnetic field increased in the compound field, the diffraction peak became increasingly sharp in the spectrum. This indicates that the crystal characteristic state of the composite coatings was increasingly evident. The related work of Xuan et al. [16] also reached a similar conclusion.

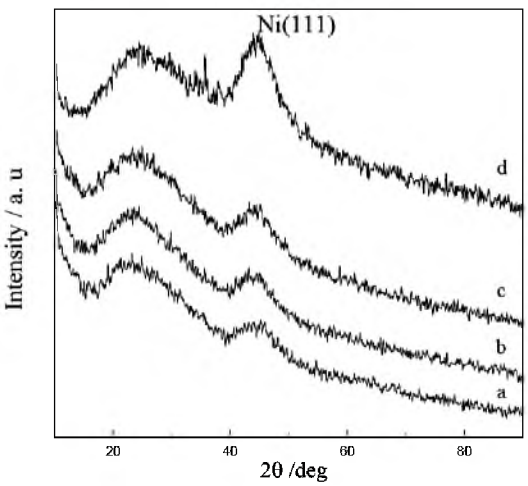

Fig. 7. XRD of composite coating samples: (a) No. 5; (b) No. 6; (c) No. 7; (d) No. 8.

The above analysis shows that when a compound field with a certain intensity was introduced to the plating, a positive effect on the deposition process, structure and morphology of the deposited products was achieved. The added ultrasound had two main effects. On the one hand, a large number of reactive free radicals could be generated in the reaction system, which could accelerate the rate of the chemical reaction [17, 18]. On the other hand, the collision probability of the Ni ions in the plating solution is increased by the ultrasonic field, which means that the Ni ions deposited on both the surface and the internal surface with catalytic activity. This helps to form uniform, compact and imporosity

composite coatings. The energy provided by the additional electromagnetic field accelerates the movement of the Ni particles in the plating solution. The Ni ions are arranged according the direction of the magnetic field lines, and the ions can be deposited directly on the substrate in this direction [19]. The added magnetic field not only promotes the codeposition of Ni and SiC, but also makes the metastable phase of the Ni-P solid solution to grow in the preferred orientation. These results agree with the results of the XRD analysis of the coating in Figs. 4 and 7.

3. **Analysis of Nanoindentation Hardness of the Coatings**. Figure 8 shows the relationship between the nanoindentation hardness and indentation depth of different composite coating samples. As can be seen from Fig. 8, the hardness values of all samples decreased as the depth increased. The hardness values stabilized when the depth exceeded 20 nm. The hardness values of samples Nos. 1 and 3 are nearly 0.50 GPa, while the hardness of samples Nos. 4, 6, and 8 is relatively low (approximately 0.15 GPa). The extra ultrasonic fields had little influence on the morphology and structure of the deposited products during the deposition process, although they could promote deposition rates. Thus, the nanoindentation hardness values of samples Nos. 1 and 3 are relatively close. On the other side, the extra electromagnetic fields promoted the formation of the orientation growing Ni-P metastable phase, which effectively reduced the average residual stress in the composite coatings. However, the Ni-P alloy coatings were not completely crystallized. Because the Ni-P metastable phase is different from that of the stable phases, such as crystal Ni_3P formed by the heat treatment, the hardness values of samples Nos. 4, 6, and 8 are lower than those of Nos. 1 and 3 samples.

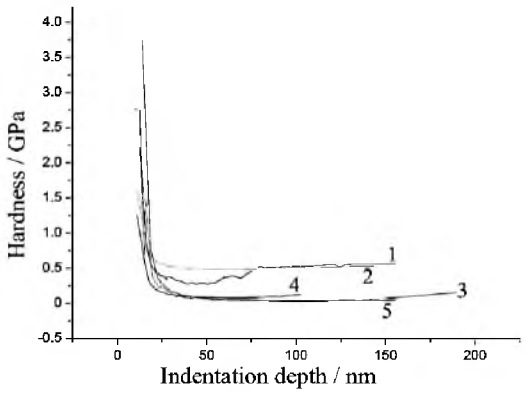

Fig. 8. Relationship between hardness and indentation depth: (*1*) No. 1, (*2*) No. 3, (*3*) No. 4, (*4*) No. 6, and (*5*) No. 8.

Conclusions. The combined fields of eletromagnetic and ultrasound waves have a significant effect on the deposition process, microstructure and the structural characteristics of electroless Ni-P based nanocomposite coatings. The Ni ions in the plating solution are arranged according to the direction of the magnetic field lines, and the ions can be deposited directly on the substrate in this direction. Thus, the added magnetic fields can make the metastable phase of the Ni-P solid solution to grow in a preferred orientation in addition to improving the deposition efficiency. The mechanical energy produced by the ultrasonic waves has a catalytic action and can accelerate the chemical reaction. As the intensity of the magnetic field increases, the density of the composite coatings also gradually increases, and the spherical deposition trend of the products and the preferred orientation growth become more obvious. Furthermore, the coatings' nanoindentation hardness values are lower than those of the coatings that were fabricated without any external fields.

Under the process conditions of nano SiC content 1 g/l, bath pH value 4.8, plating temperature 50°C, ultrasonic frequency 20 kHz and power 300 W, magnetic field strength 0.7 T, and plating time 50 min, the composite coatings are mainly composed of amorphous spherical Ni-P/SiC particles with an average size of about 200 nm. The distribution of spherical Ni-P/SiC particles is compact and uniform. Finally, the interface bonding between the coating and the glass substrate is successful.

Acknowledgments. This work is supported by the National Natural Science Foundation of China (Grant No. 51301088), the innovation practice training projects for the College students of Jiangsu Province (Grant No. 201611276053X), and the innovation practice training projects for the college students of Nanjing Institute of Technology (Grant No. TB20160227).

1. T. K. Tsai, S. J. Hsueh, J. H. Lee, and J. S. Fang, "Optical properties and durability of Al_2O_3-NiP/Al solar absorbers prepared by electroless nickel composite plating," *J. Electron. Mater.*, **41**, No. 1, 53–59 (2012).
2. G. H. Zhao, C. Ren, and Y. D. He, "Ni-P-multiwalled carbon nanotubes composite coatings prepared by mechanical attrition (MA)-assisted electroless plating," *Surf. Coat. Tech.*, **206**, Nos. 11-12, 2774–2779 (2012).
3. S. Ranganatha and T. V. Venkatesha, "Studies on the preparation and properties of electroless Ni-W-P alloy coatings and its nano-MoS_2 composite," *Phys. Scripta*, **85**, No. 3, 3560–3568 (2012).
4. L. X. Ying, Y. Liu, G. N. Liu, et al., "Preparation and properties of electroless plating wearresistant and antifriction composite coatings Ni-P-SiC-WS_2," *Rare Metal Mat. Eng.*, **44**, No. 1, 28–31 (2015).
5. Z. X. Ping, Q. Yang, C. L. Meng, et al., "Effect of mechanical attrition on microstructure and property of electroless plating Ni-P coatings on magnesium alloy," *Trans. Mater. Heat Treat.*, **29**, No. 6, 130–134 (2008).
6. V. Niksefat and M. Ghorbani, "Mechanical and electrochemical properties of ultrasonic-assisted electroless deposition of Ni-B-TiO_2 composite coatings," *J. Alloy. Compd.*, **633**, 127–136 (2015).
7. L. M. Luo, Y. C. Wu, J. Li, and Y. C. Zheng, "Preparation of nickel-coated tungsten carbide powders by room temperature ultrasonic-assisted electroless plating," *Surf. Coat. Tech.*, **206**, No. 6, 1091–1095 (2011).
8. Y. X. Lu, "Improvement of copper plating adhesion on silane modified PET film by ultrasonic-assisted electroless deposition," *Appl. Surf. Sci.*, **256**, No. 11, 3554–3558 (2010).
9. L. Zhong, L. Hou, C.-H. Liu, and Q. Ying, "Study on process and performance of electroless nickel plating nano-C60 crystals on the surface of micromechanical devices by laser-induced way," *J. Synth. Cryst.*, **40**, No. 6, 1628–1631 (2011).
10. C. Wang, Y. B. Zhong, J. Jia, et al., "Study on electro-deposited of Ni-nano-Al2O3 composites in 10 T parallel magnetic field," *J. Funct. Mater.*, **38** (S), 3562–3567 (2007).
11. V. R. Mehto and R. K. Pandey, "Activator-assisted electroless deposition of copper nanostructured films," *Int. J. Min. Met. Mater.*, **21**, No. 2, 196–203 (2014).
12. J. M. Huang, Y. Li, G. F. Zhang, et al., "Electroplating of Ni-ZrO_2 nanocomposite coating on 40CrNiMo7 alloy," *Surf. Eng.*, **29**, No. 3, 194–199 (2013).
13. S. H. Cha, H. C. Koo, and J. J. Kim, "The inhibition of silver agglomeration by gold activation in silver electroless plating," *J. Electrochem. Soc.*, **152**, No. 6, 388–391 (2005).

14. J. Ye, Q. W. Chen, H. P. Qi, and N. Tao, "Formation of nickel dendritic crystals with peculiar orientations by magnetic-induced aggregation and limited diffusion," *Cryst. Growth Des.*, **8**, No. 7, 2464–2468 (2008).
15. C. Y. Che, Y. Li, G. F. Zhang, et al., "Nanostructured Ni powder synthesized from non-aqueous bath," *Electrochemistry*, **83**, No. 4, 240–243 (2015).
16. T. P. Xuan, L. Zhang, and Q. H. Huang, "Micromorphology and wear resistance of chemical plating Co-Ni-B-Ce alloy under magnetic field," *Chin. J. Appl. Chem.*, **22**, No. 3, 268–271 (2005).
17. F. Touyeras, J. Y. Hihn, M.-L. Doche, and X. Roizard, "Electroless copper coating of epoxide plates in an ultrasonic field," *Ultrason. Sonochem.*, **8**, No. 3, 285–290 (2001).
18. F. Touyeras, J. Y. Hihn, S. Delalande, et al., "Ultrasound influence on the activation step before electroless coating," *Utrason. Sonochem.*, **10**, No. 6, 363–368 (2003).
19. X. Lyu, C. J. Wang, C. Wu, et al., "Fabrication electroless Ni-P coating under high magnetic field and thermal stability," *Hot Work. Technol.*, **43**, No. 8, 127–130 (2014).

Received 30. 08. 2016